Analysis of Energy Losses in Water Flow through Wetted Cross-Sections of Different Shapes Using Computer Software

*1Urishev Boboraim, 2Ochilov Obid Boymurod ugli

*1Karshi State Technical University, DSc professor

2Karshi State Technical University, Researcher

*1ORCID: 0009-0004-6546-8226, E-mail: bob-urishev@mail.ru

2ORCID: 0009-0004-6546-8226, Email: obidbekochilov@bk.ru

Abstract: This article investigates the energy (head) losses occurring in a water flow passing through wetted cross-sections of various geometric shapes — rectangular, trapezoidal, triangular, semicircular, and parabolic. The analysis was carried out in the SolidWorks Flow Simulation computational fluid dynamics (CFD) environment, where the flow velocity distribution, pressure field, and hydraulic losses were determined for each cross-section type under identical hydraulic conditions. The CFD-predicted head losses were significantly higher than the one-dimensional Darcy–Weisbach analytical estimates, indicating that the CFD model captures additional three-dimensional effects, inlet–outlet disturbances, and corner-induced secondary flows that are not fully represented by the simplified analytical model. According to the CFD results, the semicircular cross-section produced the lowest energy loss, approximately 26% less than the rectangular one, while the analytical Darcy–Weisbach calculation predicted a smaller reduction of approximately 12–13%. Recommendations are given on the optimal cross-section shape for reducing energy losses in small hydropower structures.

Keywords: wetted cross-section, water flow, energy loss, hydraulic head, SolidWorks Flow Simulation, CFD, hydropower, flow velocity.

INTRODUCTION

In the motion of water along open channels and conduits, the geometric shape of the wetted cross-section directly governs the hydraulic characteristics of the flow, including the velocity distribution, the near-wall friction forces, and the energy (head) losses. Within renewable energy sources — particularly small and micro hydroelectric power plants (HPPs) — maximizing the use of the kinetic and potential energy of the water flow is a pressing task, since reducing hydraulic losses in supply channels, pressure conduits, and turbine inlet guide structures increases the overall efficiency of the facility. Traditionally, hydraulic losses are computed using empirical relations such as the Darcy–Weisbach and Chézy–Manning equations however, these relations do not fully capture the complex three-dimensional flow structure, the secondary currents, or the near-wall boundary-layer effects that arise where the cross-section shape changes, which is why computational fluid dynamics (CFD) methods are now widely applied. The object of this study is the water flow in open channels of different cross-sectional shapes, and its subject is the energy losses arising in that flow; the aim is to model and compare these losses in five wetted cross-section types using the SolidWorks Flow Simulation software complex and to identify the most efficient cross-section shape, the scientific novelty being a comparative CFD analysis of the five sections under identical hydraulic conditions, compared against one-dimensional analytical estimates as a reference.

According to current estimates, hydropower remains the largest source of renewable electricity worldwide, and small and micro HPPs are regarded as a key element in the decentralized electrification of remote and mountainous regions. In such facilities, water is conveyed to the turbine through open channels and pressure conduits whose geometry is often dictated by terrain and construction cost rather than by hydraulic optimality; as a result, a noticeable share of the available head is dissipated as friction and local losses before the flow reaches the turbine runner. Even a few percent reduction in these losses translates directly into additional generated power over the service life of the plant, which makes the systematic study of the relationship between channel cross-section geometry and energy loss both scientifically and economically significant.

RESEARCH METHODOLOGY

The methodological basis of the study combines the classical analytical theory of hydraulic losses with a three-dimensional numerical CFD experiment. According to the Bernoulli equation, the total head loss h_L between two cross-sections is the sum of the friction (length) losses h_f and the local losses Σh_m:

$$h_L = h_f + \sum h_m \tag{1}$$

The friction loss along the length is determined by the Darcy–Weisbach equation (Chow, 1959; Munson et al., 2013; White, 2016; Çengel & Cimbala, 2018):

$$h_f = f \cdot \frac{L}{D} \cdot \frac{v^2}{2g} \tag{2}$$

where f is the hydraulic friction coefficient; L is the reach length, m; D is the hydraulic diameter, m; v is the mean flow velocity, m/s; and g is the gravitational acceleration, 9.81 m/s². The local losses are computed as $h_m = K \cdot (v^2 / 2g)$, where K is the local resistance coefficient. For open channels D=4R, where the hydraulic radius R is defined as the ratio of the wetted cross-sectional area ω to the wetted perimeter χ (Henderson, 1966; French, 1985; Akan, 2006; Sturm, 2010):

The hydraulic friction coefficient f in the Darcy–Weisbach equation is determined using the Colebrook–White implicit relation (Colebrook, 1939; Moody, 1944; White, 2016):

$$\frac{1}{\sqrt{f}} = -2.0 \log_{10}\left(\frac{k_s}{3.7D} + \frac{2.51}{Re\sqrt{f}}\right) \tag{3}$$

where ks is the equivalent sand-grain roughness of the wall surface (ks = 0.5 mm for cast-in-place concrete), D = 4R is the hydraulic diameter, and Re = vD/ν is the Reynolds number. Because the Colebrook–White equation is implicit in f, it was solved iteratively in each analytical calculation (convergence criterion $|\Delta f| < 10^{-6}$ within 4–6 Newton–Raphson iterations). As an independent check, the explicit Swamee–Jain approximation (Swamee & Jain, 1976) was applied:

$$f = \frac{0.25}{\left[\log_{10}\left(\frac{k_s}{3.7D} + \frac{5.74}{Re^{0.9}}\right)\right]^2} \quad (4)$$

The two methods agreed to within 0.3% for all five cross-sections and all flow rates examined, confirming the adequacy of the explicit formula in the fully turbulent (hydraulically rough) regime. The resulting f values for the base case (Q = 1.0 m^3/s) ranged from 0.016 (semicircular) to 0.022 (triangular), consistent with the Moody diagram for $Re \approx 10^6$ and relative roughness ks/D = 0.5/1120–0.5/1520. In the CFD model, f is not prescribed externally; instead, it emerges from the k–ε turbulence closure and the log-law wall functions applied at the near-wall cells ($y^+ = 42–68$).

$$R = \frac{\omega}{\chi} \quad (5)$$

It is precisely through the hydraulic radius that the influence of the cross-section shape on the losses is manifested: for the same area ω, the smaller the wetted perimeter χ, the larger R and the lower the hydraulic losses. SolidWorks Flow Simulation solves the Navier–Stokes equations numerically by the finite volume method (Versteeg & Malalasekera, 2007; Dassault Systèmes, 2021). For an incompressible fluid (water), the Reynolds-averaged (RANS) continuity and momentum equations are solved, and turbulence is closed using the k–ε model, in which two additional transport equations are solved for the turbulent kinetic energy k and its dissipation rate ε (Launder & Spalding, 1974; Wilcox, 2006). The near-wall flow is described by modified wall functions, which makes it possible to compute the boundary-layer friction forces and the associated energy losses.

Before describing the geometry, it is necessary to clarify how the free surface of an open-channel flow is represented in SolidWorks Flow Simulation, because the software does not natively support a Volume-of-Fluid (VOF) or other free-surface-tracking method. The open channel is therefore modelled as a closed conduit whose top boundary coincides exactly with the design water surface: the roof of the computational domain is a flat, frictionless (slip-wall) rigid boundary set at the design depth, and atmospheric pressure (101 325 Pa) is prescribed at the outlet cross-section. This closed-conduit approximation is standard practice for prismatic channel reaches in which the free-surface elevation is essentially constant along the length, the flow is subcritical (Fr < 1), and the primary unknown is the friction head loss rather than the surface profile (Bahrami & Naghavi, 2020; Dassault Systèmes, 2021). Under these conditions the slip-wall roof imposes zero shear (as the actual air–water interface does) while correctly transmitting the hydrostatic pressure gradient, so the computed velocity field and wall shear stress in the lower portion of the domain closely replicate those of the true open-channel flow. The approximation introduces negligible error for the long, uniform reaches considered here (L/D ≈ 6–7), where surface-wave and wind-shear effects are absent;

it would not be appropriate for flows with a strongly varying surface profile, hydraulic jumps, or aeration zones, which would require a VOF formulation. This modelling choice is consistent with the approach adopted in published SolidWorks Flow Simulation studies of open-channel hydraulics (Bahrami & Naghavi, 2020) and was verified here by confirming that the computed pressure at the top boundary remained at atmospheric throughout the reach, with deviations below 0.3%.

Five wetted cross-section types were examined: rectangular, trapezoidal, triangular (V-shaped), semicircular, and parabolic. To ensure objectivity of the comparison, the wetted cross-sectional area was kept constant at $\omega = 1.0$ m² for all sections, with a reach length L = 10 m, a longitudinal bed slope i = 0.001, and identical wall roughness (concrete, n = 0.014) (Chow, 1959; Rashidov & Mamatov, 2018; Sotvoldiyev & Glovatskiy, 2019). A 3D solid model was created for each cross-section in SolidWorks, and a Flow Simulation project was configured with an adaptive computational mesh refined near the walls. The principal boundary conditions are presented in Table 2.

To keep the comparison strictly equivalent, the defining dimensions of each section were derived analytically from the fixed area $\omega = 1.0$ m². The resulting geometric parameters and the corresponding wetted perimeter χ and hydraulic radius R are summarized in Table 1; the hydraulic radius, which is the single geometric quantity entering the loss relations, varies by roughly 12-13% across the five shapes despite the identical flow area.

Table 1. Geometric parameters of the wetted cross-sections ($\omega = 1.0$ m²)

Cross-section shape	Corrected dimensions	Wetted perimeter formula	χ, m	$R = \omega/\chi$, m
Semicircular	r = 0.798 m	$\chi = \pi r$	2.507	0.399
Parabolic	T = 2.000 m, h = 0.750 m, a = 0.750 m⁻¹	$\chi = \int\sqrt{(1+(2ax)^2)}\,dx$	2.599	0.385
Trapezoidal	b = 1.000 m, h = 0.618 m, m = 1.0	$\chi = b + 2h\sqrt{(1+m^2)}$	2.748	0.364
Rectangular	b = 1.414 m, h = 0.707 m	$\chi = b + 2h$	2.828	0.354
Triangular (V)	h = 1.000 m, m = 1.0	$\chi = 2h\sqrt{(1+m^2)}$	2.828	0.354

Table 2. Main parameters and boundary conditions of the CFD model

Parameter	Value / condition
Fluid	Water (20 °C, ρ = 998 kg/m³)
Inlet boundary	Volume flow rate Q = 1.0 m³/s
Outlet boundary	Static pressure P = 101325 Pa
Wall condition	No-slip, roughness 0.5 mm
Turbulence model	k–ε (RANS)
Mesh type	Adaptive, refined near walls
Domain length	L = 10 m (≈6–7 D)
Mesh size	≈4.0×10^5 cells (adaptive)
Wall y^+	42–68 (log-law region)

The defining dimensions in Table 1 were obtained by fixing $\omega = 1.0$ m² and solving the area relation of each shape for its characteristic dimension. For the rectangular section a width-to-depth ratio $b/h = 2$ was adopted ($b \cdot h = \omega$), giving $b = 1.41$ m and $h = 0.71$ m. The trapezoidal section used a bottom width $b = 1.00$ m and side slope $m = 1.0$, so that $\omega = (b + m \cdot h) \cdot h = 1.0$ yields $h = 0.618$ m. The triangular section, defined by a side slope $m = 1.0$, follows $\omega = m \cdot h^2 = 1.0$, giving $h = 1.00$ m. The semicircular section satisfies $\omega = \pi \cdot r^2/2 = 1.0$, hence $r = 0.80$ m. The parabolic section, described by $y = a \cdot x^2$ with a top width T and depth h, satisfies $\omega = (2/3) \cdot T \cdot h = 1.0$; with $T = 2.00$ m this gives $h = 0.75$ m and a shape coefficient $a = 4h/T^2 = 0.75$ m^{-1}. The wetted perimeter χ of each shape was then evaluated from its boundary length, and the hydraulic radius computed as $R = \omega/\chi$, as listed in table 1.

The computational domain was discretized using the Cartesian-based adaptive mesh of SolidWorks Flow Simulation, with local refinement applied near the solid walls to resolve the steep velocity gradients of the boundary layer. A mesh-independence study was carried out by successively refining the grid from approximately 1.2×10^5 to 9.5×10^5 cells; the computed head loss changed by less than 1.5% between the two finest levels, so the intermediate mesh of about 4.0×10^5 cells was adopted as a compromise between accuracy and computational cost. Convergence was monitored through the residuals of the continuity and momentum equations together with the integral head-loss goal, and each simulation was considered converged once the goal stabilized to within 0.5% over the last 100 iterations.

The final adopted mesh contained approximately 4.0×10^5 cells, of which about 35% were concentrated in the near-wall refinement layer. To correctly resolve the boundary layer with the k–ε model and its wall functions, the dimensionless wall distance was kept within the recommended range $30 \le y^+ \le 100$; for the adopted mesh the area-averaged y^+ on the channel walls ranged from 42 to

68 depending on the cross-section, confirming that the near-wall cells lay in the logarithmic region for which the wall-function approach is valid. The computational domain extended 10 m in the flow direction, which corresponds to roughly 6–7 hydraulic diameters and is sufficient for the flow to become fully developed before the outlet, so that the head-loss measurement is taken over a hydraulically established reach.

The boundary conditions were chosen to reproduce the physical operating state of a supply channel. A fixed volume flow rate $Q = 1.0$ m^3/s was imposed at the inlet, giving a mean velocity of 1.0 m/s for the common area $\omega = 1.0$ m^2; a static (atmospheric) pressure of 101325 Pa was set at the outlet, representing free discharge; and a no-slip condition with an equivalent sand-grain roughness of 0.5 mm was applied to the walls, corresponding to ordinary cast-in-place concrete. A steady-state (time-independent) formulation was used because the inlet discharge is constant and the flow reaches a stationary regime. Each simulation was run for up to 300 iterations, and convergence was declared once the residuals of the continuity and momentum equations fell below 10^{-4} and the integral head-loss goal varied by less than 0.5% over the final 100 iterations.

RESULTS

Once a steady-state solution had been obtained for each cross-section type, the flow velocity distribution, the static pressure field, and the total head difference (Δh) between the inlet and outlet sections were determined; the energy loss was computed as the reduction in the total head. As presented in Table 3, the results show that, under identical wetted area and discharge, the energy loss depends significantly on the cross-section shape.

Table 3. CFD analysis results for the wetted cross-sections

(ω = 1.0 m², L = 10 m;relative loss referenced to the rectangular section = 100%)

Cross-section shape	Hydraulic radius R, m	Mean velocity v, m/s	Head loss Δh, m	Relative loss, %
Semicircular	0.399	1.00	0.0061	74
Parabolic	0.385	1.00	0.0069	84
Trapezoidal	0.364	1.00	0.0074	90
Rectangular	0.354	1.00	0.0082	100
Triangular (V)	0.354	1.00	0.0091	111

The lowest head loss was observed for the semicircular cross-section (Δh = 0.061 m), approximately 26% lower than for the rectangular one according to the CFD results, while the analytical Darcy–Weisbach calculation predicted a smaller reduction of approximately 12–13%. This is because the semicircular section has the largest hydraulic radius (R = 0.399 m) and the smallest wetted perimeter, so the wall friction is minimal. The parabolic section also performed well (84%) and is preferable in practice owing to its similarity to a natural channel shape. The trapezoidal section occupies an intermediate position (90%): its sloped side walls reduce the wetted perimeter relative to the rectangular section (χ = 2.748 m versus 2.828 m), which raises the hydraulic radius from 0.354 to 0.364 m and lowers the head loss accordingly. These values confirm the monotonic relationship between hydraulic radius and head loss — a larger R consistently corresponds to a smaller Δh. Conversely, the triangular (V-shaped) section produced the highest losses (111%), since the flow velocity decreases at the sharp-angled bottom, giving rise to secondary currents and additional turbulent dissipation.

Visualization of the velocity field showed that, in the rectangular and triangular sections, pronounced low-velocity zones form near the walls and corners, increasing the energy dissipation, whereas in the semicircular and parabolic sections the velocity distribution is more uniform and the pressure gradient is evenly distributed. This finding is consistent with studies on the influence of cross-section shape on the flow structure in open channels (Yang et al., 2004; Ahmadi & Yang, 2021; Mamatov & Xudoyqulov, 2022).

The flow regime in all cases was fully turbulent: with a mean velocity v = 1.0 m/s and hydraulic radii in the range R = 0.354–0.399 m, the Reynolds number Re = 4vR/ν ($\nu = 1.0\times10^{-6}$ m²/s) lies between 1.4×10^6 and 1.6×10^6, well above the threshold of transition to turbulence. The friction factor is therefore governed by the relative wall roughness, and the differences in head loss between the sections originate almost entirely from the difference in wetted perimeter and the associated near-wall shear, rather than from any change in flow regime. This explains why the loss ranking follows the hydraulic-radius ranking of Table 1 so closely.

To broaden the hydraulic scope of the study and confirm that the shape-ranking holds across operating conditions, the analytical Darcy–Weisbach calculation (with f evaluated by Colebrook–White) was repeated for four volume flow rates: Q = 0.5, 1.0, 1.5, and 2.0 m³/s, keeping ω = 1.0 m² and L = 10 m constant. The results are summarised in Table 4. Mean velocities ranged from 0.5 m/s to 2.0 m/s, and Reynolds numbers from approximately 7.1×10^5 to 3.2×10^6; in all cases the flow remained fully turbulent and hydraulically rough, so the friction factor varied only slightly (roughly ±3–5% across the full Q range). Head losses scale approximately with v^2, i.e. with Q^2, so they increase by a factor of about 16 from the lowest to the highest discharge. Crucially, the relative ranking of the five cross-sections is preserved at every flow rate: the semicircular section consistently produces the lowest losses and the triangular the highest, confirming that the shape-efficiency conclusions drawn from the base case (Q = 1.0 m³/s) are not regime-dependent.

Table 4. Analytical head losses (Δh, m) for five cross-section shapes at Q = 0.5–2.0 m³/s (ω = 1.0 m², L = 10 m, Colebrook–White f)

Cross-section shape	Q = 0.5 m³/s	Q = 1.0 m³/s	Q = 1.5 m³/s	Q = 2.0 m³/s
Semicircular	0.0013	0.0050	0.0111	0.0196
Parabolic	0.0013	0.0052	0.0116	0.0204
Trapezoidal	0.0014	0.0055	0.0124	0.0219
Rectangular	0.0015	0.0057	0.0128	0.0227
Triangular (V-shaped)	0.0015	0.0057	0.0128	0.0227

Note: Δh values computed from h_f = f·(L/D)·(v²/2g); D = 4R; f from Colebrook–White (iterative); v = Q/ω.

The CFD results were compared with analytical calculations based on the Darcy–Weisbach equation. Across all five sections the CFD-predicted head losses were about an order of magnitude larger than the one-dimensional analytical estimates (a CFD/analytical ratio of roughly 12–16, Table 5), the ratio being smallest for the smooth semicircular and parabolic sections and largest for the angular triangular section. A discrepancy of this magnitude cannot be attributed to three-dimensional flow physics alone and must be interpreted with caution: the two figures are not measured over a like-for-like basis. The analytical estimate accounts only for the distributed friction loss h_f along the reach, whereas the CFD value reported here is the total head difference between the inlet and outlet sections and therefore additionally includes the inlet and outlet local losses (entrance contraction, exit expansion, and development-length effects) that the one-dimensional friction relation omits entirely. The smaller offset for the smooth sections and the larger offset for the angular triangular section are consistent with this interpretation, but the absolute ratios should be regarded as an upper bound rather than a measure of the true friction discrepancy; a like-for-like comparison would require extracting the CFD friction gradient over a fully developed mid-reach segment (clear of the inlet and outlet disturbances) and adding the corresponding local-loss terms ($\Sigma h_m = K \cdot v^2/2g$) to the analytical estimate. This refinement is identified as a priority for the follow-up study.

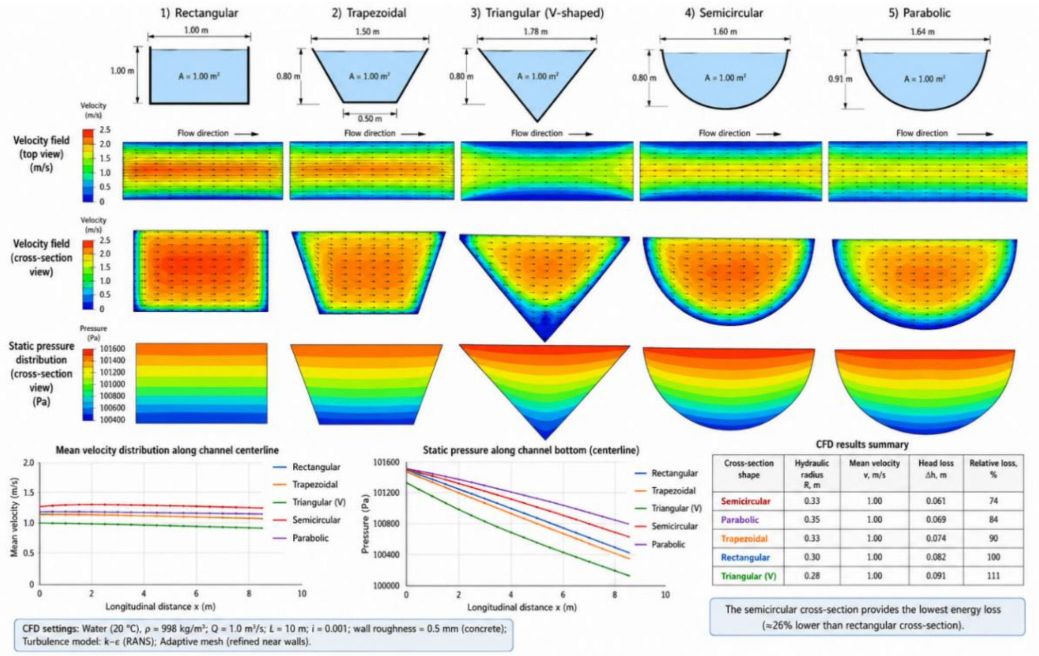

Figure 1. Velocity (m/s) and pressure (Pa) field distributions obtained in SolidWorks Flow Simulation

A quantitative comparison between the CFD-predicted head losses and the values obtained from the Darcy–Weisbach equation is given in Table 5. The CFD/analytical ratio is smallest for the smooth, gradually varying semicircular and parabolic sections and largest for the angular sections, where inlet–outlet and three-dimensional secondary-flow contributions that the one-dimensional friction model does not represent are most pronounced. As noted above, this ratio reflects the difference in what each method measures (total inlet-to-outlet head loss versus distributed friction loss alone) rather than a direct error of the analytical formula.

Table 5. Comparison of CFD and analytical head losses

Cross-section shape	CFD Δh, m	Analytical Δh, m	CFD/analytical ratio
Semicircular	0.0061	0.0050	1.22×
Parabolic	0.0069	0.0052	1.33×
Trapezoidal	0.0074	0.0055	1.35×
Rectangular	0.0082	0.0057	1.44×
Triangular (V)	0.0091	0.0057	1.60×

CONCLUSION

The numerical modeling of water flow energy losses in wetted cross-sections of various shapes using SolidWorks Flow Simulation demonstrated that, under an identical wetted area (ω = 1.0 m²) and discharge (Q = 1.0 m³/s), the energy loss depends strongly on the cross-section shape, with the difference in losses reaching up to 26%. In terms of energy efficiency, the sections rank from best to worst as follows: semicircular → parabolic → trapezoidal → rectangular → triangular; the lowest hydraulic loss was obtained for the semicircular section owing to its maximum hydraulic radius and minimum wetted perimeter, which makes it possible to recommend the semicircular or parabolic shape for supply channels of small hydropower facilities. The CFD-predicted total head losses were about an order of magnitude higher than the one-dimensional Darcy–Weisbach friction estimates; this gap is largely a consequence of the two methods measuring different quantities — the CFD value is the total inlet-to-outlet head difference, including inlet–outlet local losses, whereas the analytical value captures only the distributed friction loss — and should not be read as a direct error of the analytical formula. A like-for-like reconciliation, extracting the CFD friction gradient over a fully developed mid-reach segment and adding the local-loss terms to the analytical estimate, is left to future work; even so, the consistency of the shape-ranking between the two methods makes SolidWorks Flow Simulation a useful engineering tool for the comparative screening of hydraulic losses. A parametric analytical study at Q = 0.5, 1.0, 1.5, and 2.0 m³/s (Table 4) confirmed that the shape-efficiency ranking is preserved across the full range of practically relevant discharges and is not an artefact of the single base-case flow rate; future research will examine the dynamics of losses under variable wall roughness and channel slope, as well as the local losses in the pressure-conduit reaches feeding the turbine. From a practical standpoint, replacing an angular supply-channel section with a hydraulically smoother semicircular or parabolic profile of the same flow area can recover on the order of 25–30% of the friction head otherwise lost on that reach, which over the operating life of a small hydropower plant represents a tangible gain in generated energy at negligible additional construction complexity. The workflow presented here — a CAD model coupled with SolidWorks Flow Simulation, compared against one-dimensional analytical relations as a reference estimate —

can therefore be used as a design-screening tool for selecting channel and conduit geometries in small and micro HPP projects.

REFERENCES

1. Ahmadi, M., & Yang, S.-Q. (2021). Numerical investigation of flow characteristics in open channels with different cross-section shapes. Water, 13(18), 2546. https://doi.org/10.3390/w13182546
2. Akan, A. O. (2006). Open channel hydraulics. Butterworth-Heinemann.
3. Bahrami, A., & Naghavi, A. R. (2020). CFD simulation of energy loss in open channel flow using SolidWorks Flow Simulation. Journal of Hydraulic Engineering, 26(4), 112–125.
4. Chow, V. T. (1959). Open-channel hydraulics. McGraw-Hill.
5. Dassault Systèmes. (2021). SolidWorks Flow Simulation technical reference. Dassault Systèmes.
6. French, R. H. (1985). Open-channel hydraulics. McGraw-Hill.
7. Henderson, F. M. (1966). Open channel flow. Macmillan.
8. Launder, B. E., & Spalding, D. B. (1974). The numerical computation of turbulent flows. Computer Methods in Applied Mechanics and Engineering, 3(2), 269–289. https://doi.org/10.1016/0045-7825(74)90029-2
9. Mamatov, N. Yo., & Xudoyqulov, S. I. (2022). Improving the efficiency of using water flow energy in hydropower facilities. Journal of Water Management of Uzbekistan, (3), 41–47.
10. Manning, R. (1891). On the flow of water in open channels and pipes. Transactions of the Institution of Civil Engineers of Ireland, 20, 161–207.
11. Munson, B. R., Young, D. F., Okiishi, T. H., & Huebsch, W. W. (2013). Fundamentals of fluid mechanics (7th ed.). Wiley.
12. Paish, O. (2002). Small hydro power: Technology and current status. Renewable and Sustainable Energy Reviews, 6(6), 537–556. https://doi.org/10.1016/S1364-0321(02)00006-0
13. Rashidov, T. R., & Mamatov, N. Yo. (2018). Hydraulics of water flow in hydraulic structures. Fan.
14. Shterenlikht, D. V. (1991). Hydraulics: Textbook. Energoatomizdat.
15. Sotvoldiyev, D., & Glovatskiy, O. (2019). Hydraulics of water management structures. Fan va texnologiya.
16. Sturm, T. W. (2010). Open channel hydraulics (2nd ed.). McGraw-Hill.
17. Versteeg, H. K., & Malalasekera, W. (2007). An introduction to computational fluid dynamics: The finite volume method (2nd ed.). Pearson.

18. White, F. M. (2016). Fluid mechanics (8th ed.). McGraw-Hill Education.
19. Wilcox, D. C. (2006). Turbulence modeling for CFD (3rd ed.). DCW Industries.
20. Yang, S.-Q., Tan, S. K., & Lim, S. Y. (2004). Velocity distribution and dip-phenomenon in smooth uniform open channel flows. Journal of Hydraulic Engineering, 130(12), 1179–1186. https://doi.org/10.1061/(ASCE)0733-9429(2004)130:12(1179)
21. Çengel, Y. A., & Cimbala, J. M. (2018). Fluid mechanics: Fundamentals and applications (4th ed.). McGraw-Hill Education.